Acta Radiologica Open
6(8) 1–10

DOI: 10.1177/2058460117718407
journals.sagepub.com/home/arr
SAGE

Two novel direct SPIO labels and in vivo MRI detection of labeled cells after acute myocardial infarct

Riikka M Korpi[1,2], Kirsi Alestalo[3,4], Timo Ruuska[4], Eveliina Lammentausta[1], Ronald Borra[5,6], Fredrik Yannopoulos[3], Siri Lehtonen[7], Jarkko T Korpi[8], Elisa Lappi-Blanco[9], Vesa Anttila[3], Petri Lehenkari[3,4], Tatu Juvonen[3,10] and Roberto Blanco Sequieros[1,11]

Abstract

Background: Acute myocardial infarction (AMI) is a leading cause of morbidity and mortality worldwide. Cellular decay due hypoxia requires rapid and validated methods for possible therapeutic cell transplantation.
Purpose: To develop direct and rapid superparamagnetic iron oxide (SPIO) cell label for a large-animal model and to assess in vivo cell targeting by magnetic resonance imaging (MRI) in an experimental AMI model.
Material and Methods: Bone marrow mononuclear cells (BMMNCs) were labeled with SPIO particles using two novel direct labeling methods (rotating incubation method and electroporation). Labeling, iron incorporation in cells and label distribution, cellular viability, and proliferation were validated in vitro. An AMI porcine model was used to evaluate the direct labeling method (rotating incubation method) by examining targeting of labeled BMMNCs using MRI and histology.
Results: Labeling (1 h) did not alter either cellular differentiation potential or viability of cells in vitro. Cellular relaxation values at 9.4 T correlated with label concentration and MRI at 1.5 T showing $89 \pm 4\%$ signal reduction compared with non-labeled cells in vitro. In vivo, a high spatial correlation between MRI and histology was observed. The extent of macroscopic pathological myocardial changes (hemorrhage) correlated with altered function detected on MRI.
Conclusion: We demonstrated two novel direct SPIO labeling methods and demonstrated the feasibility of clinical MRI for monitoring targeting of the labeled cells in animal models of AMI.

Keywords

Magnetic resonance imaging (MRI), acute myocardial infarct (AMI), superparamagnetic iron oxide (SPIO) particles, bone marrow mononuclear cells (BMMNCs), transplantation

Date received: 4 November 2016; accepted: 8 June 2017

[1]Department of Diagnostic Radiology, University of Oulu and Oulu University Hospital, Oulu, Finland
[2]Department of Radiology, Helsinki University Hospital, Helsinki, Finland
[3]Department of Surgery and Clinical Research Center, University of Oulu and Oulu University Hospital, Oulu, Finland
[4]Department of Anatomy and Cell Biology, University of Oulu, Oulu, Finland
[5]Medical Imaging Center of Southwest Finland, Turku University Hospital, Turku, Findland
[6]A.A. Martinos Center for Biomedical Imaging, Massachusetts General Hospital, Boston, MA, USA
[7]MRC Oulu and Department of Obstetrics and Gynecology, Oulu University Hospital and PEDEGO Research Unit, University of Oulu, Oulu, Finland
[8]Department of Otorhinolaryngology, Head and Neck Surgery, Helsinki University Hospital, Helsinki, Finland
[9]Department of Pathology, University of Oulu and Oulu University Hospital, Oulu, Finland
[10]Department of Cardiac Surgery, HUCH Heart and Lung Center, Helsinki, Finland
[11]Department of Radiology, University of Turku and Turku University Hospital, Turku, Finland

Corresponding author:
Riikka M. Korpi, Department of Diagnostic Radiology, Institute of Medicine, University of Oulu, P.O. BOX 5000, Oulu 90014, Finland.
Email: riikka.korpi@hus.fi

Introduction

Acute myocardial infarction (AMI) is the most common cause of death worldwide (1) and current therapeutic strategies aim to establish revascularization (2). Administration of bone marrow cells has emerged as a potential candidate for cardiac tissue repair or as a paracrine modulator of healing after AMI in both non-clinical (3–6) and clinical studies (7,8), though the clinical results remain controversial.

In AMI tissue repair, cell transplantation has to be administered promptly in order to minimize cellular decay due hypoxia. Hence, rapid and validated in vivo methods are needed for cellular labeling and visualization of transplanted cells. Most imaging related stem cell studies have employed bone marrow cells due to their ease of harvest, multi-lineage potential (9–11), immunological advantages, and potential therapeutic effect in AMI (3–6).

Cell tracking in vivo is crucial for the development of novel therapies that require precise targeting of the therapeutic agent (12,13). Contrast-enhanced magnetic resonance imaging (MRI) is the gold standard for non-invasive evaluation of myocardial pathology. MRI is a suitable technique for monitoring cell migration in vivo, cell distribution after transplantation (14,15), and for evaluating the post-transplantation regenerative effect in cardiac tissue (16). Among the different MRI contrast agents, superparamagnetic iron oxide (SPIO) particles are low in toxicity, offer a relatively simple, inexpensive, non-invasive, and currently the most sensitive method for detecting labeled cells at micromolar concentrations in T2(*)-weighted (T2(*)W) MRI (15).

In SPIO labeling, the cells are incubated with SPIO particles inducing endocytosis of a contrast agent (17). SPIO particles have been used in a variety of cell labeling AMI protocols (17) but rather few in large animals (6,18,19). In general, the effects of the label have been fairly well described (15). However, typical cellular labeling times of 48 h are used, thus introducing a potential problem of reaching a clinically feasible time margin for cell transplantation in the acute setting. Permeabilization agents may be used to enhance cell labeling but they are potentially toxic (20). Based on earlier reports (21,22), we hypothesized that clinically sufficient labeling of BMMCs could be achieved without the use of transfection agents or prolonged exposure times via receptor-mediated intake of SPIO by using a carboxydextran-coated SPIO contrast agent and by using either the rotating incubation method or electroporation. Electroporation induces the intra-cellular intake of SPIO particles making possible a more rapid clinical translation. The rotating incubation method also potentially expedites intake of label through the motion-related interaction of label and cells and additionally the inhibition of cell adherence seems to increase label intake by some unknown mechanism, although one probably linked to increased cellular stress and induced pinocytosis.

This study aimed to demonstrate two direct and fast in vitro SPIO labeling methods for MRI and further characterize targeting of labeled bone marrow mononuclear cells (BMMNCs) in an AMI model.

Material and Methods

Animals

An animal experiment was approved by the National Animal Experiment Board (ESLH-2007-09818/Ym-23). Three 56–70-day-old landrace pigs were anesthetized as previously described (23). Briefly, the pigs were anesthetized with ketamine hydrochloride (Pfizer AB, Sollentuna, Sverige) and midazolam (Pfizer AB), and balanced anesthesia was maintained with fentanyl (Fentanyl-Hameln, Hameln, Germany), midazolam (Pfizer AB), pancuronium (0.2 mg/kg/h) (Hameln), and inhaled isoflurane (Orion Pharma, Turku, Finland).

Isolation and culture of cells

The bone marrow aspirate from the tibial tuberosity was subjected to a density-gradient centrifugation (Ficoll-Paque Plus, GE Healthcare Bio-Sciences AB, Uppsala, Sweden) to exclude granulocytes and erythrocytes. Harvested BMMNCs were washed three times with phosphate buffered saline (PBS) and plated. BMMNCs were collected and expanded in culture.

SPIO labeling

After piloting various concentrations, in the in vitro model, SPIO labeling (labeling time 1 h) was performed using 0.1 and 0.2 mg/mL concentrations of the organ-specific MRI contrast agent that consists of SPIO particles coated with carboxydextran, (Resovist, Bayer Healthcare, Berlin, Germany). Two labeling methods were used: 1 = a rotating incubation method, where BMMNCs were incubated with the samples being rotated continuously to prevent aggregation; and 2 = electroporation, where BMMNCs were suspended in a sterile electroporation cuvette and mixed with the label and electroporated with two square wave protocols (100 V for duration of 10 ms and 100 V 5×100 V for 10 ms). Subsequently, the cells in cuvettes were transferred to ice and washed with PBS. Control BMMNCs were incubated with basal medium without label. Labeled BMMNCs were suspended into an agarose gel (10^8cells/1 mL).

In the infarct model, SPIO labeling was done as previously described (6). Briefly, the rotating incubation method with 39 mg/mL ferucarbotran corresponding to 36 mM iron (Resovist, Bayer Healthcare) was used.

Infarct model

An AMI was induced as previously described (23). Briefly, the circumflex coronary artery (CCA) was surgically coiled with a removable silicone vascular loop (Surg-I-Loop, Scanlan, St. Paul, MN, USA) for 90 min.

Next, the labeled BMMNCs (10^8/2 mL) were transplanted randomly into five different locations within the territory vascularized by CCA by direct surgical intramuscular injections (26-gauge needle, depth = 5–10 mm). After 1 h, pigs were MRI scanned in vivo, sacrificed, and cardiac tissue was prepared and fixed with 10% formaldehyde. After 24 h, myocardial tissue was ex vivo MRI scanned and prepared for histology. The left ventricle was divided into 16 segments according to a standardized myocardial segmentation scheme (24). The tissue sections (5 mm) were excised continuously through the left ventricle along with the short axes of the left ventricle (resulting in three sections per segment), paraffin embedded, and stained with Prussian blue as previously described (25).

MRI

MRI was performed in vitro, in vivo, and ex vivo to validate the labeling success (in vitro), to study how well MRI images matched with histology (in vivo) and the correlation between in vivo and ex vivo MRI.

In vitro imaging: We utilized a 9.4 T Oxford NMR vertical magnet (Oxford Instruments, Abingdon, UK), Varian Direct Drive console (Varian Associates Inc., Palo Alto, CA, USA), and 1.5 T MRI scanner (GE Signa Twinspeed, GE Healthcare, Milwaukee, WI, USA).

At 9.4 T (Oxford Instruments), spectroscopic T1, T2, and T2* relaxation times were measured using a 10 mm spectroscopy probe. T1 was calculated from peak

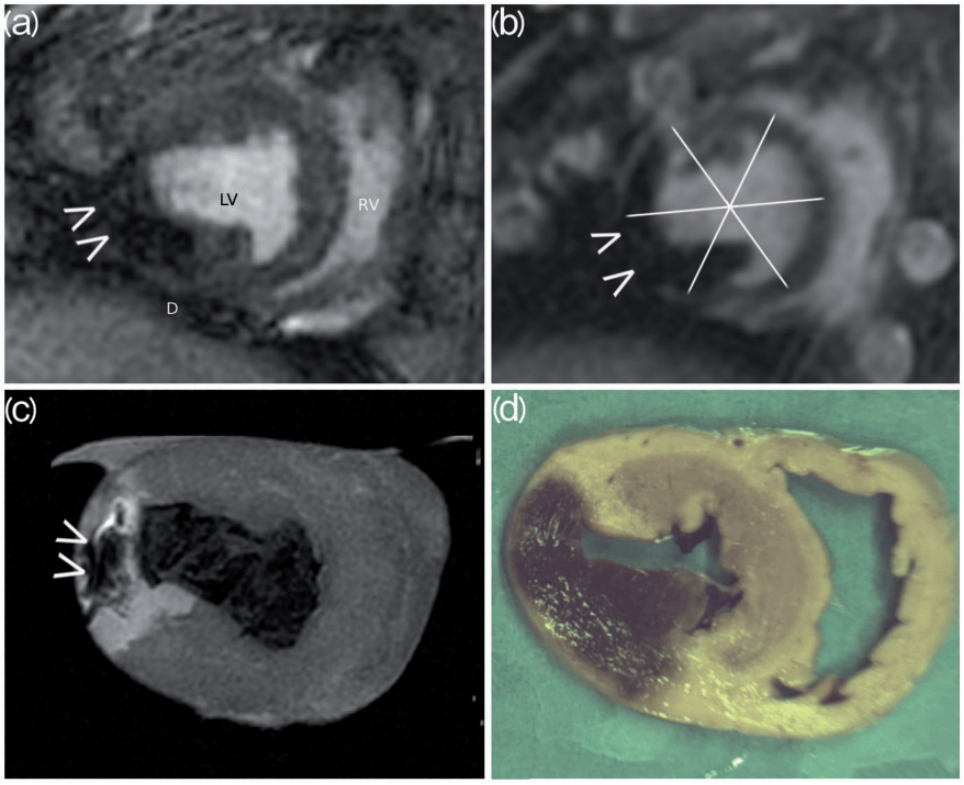

Fig. 1. Localization of labeled BMMNCs in infarcted myocardium. (a) Hypo-intensity caused by SPIO-labeled cell accumulation in a short axis view (arrows) at 1.5 T. (b) Hypo-intensity caused by SPIO-labeled BMMNCs in a DE image (arrows) at 1.5 T. (c) SPIO-labeled BMMNCs in an ex vivo T2 FSE image at 1.5 T. Intramyocardial hemorrhage in the infarcted area results in a high signal intensity when combined with a SPIO-label-induced area of hypointensity (arrows). (d) Intramyocardial hemorrhage visible on a macroscopic slice of the myocardial tissue. ROI-based method was used to define each segmental area; a simplified diagram of the segmental scheme is provided to clarify the segmentation (24); this is placed on top of the figure (b). LV, left ventricle; RV, right ventricle; D, diaphragm.

values/areas of the spectra obtained using an inversion recovery sequence (repetition time [TR] = 7000 ms, echo time [TE] = 2 ms, 11 inversion time [TI] in the range of 5–5000 ms). T2 relaxation time was measured using a spin echo (SE) (TR = 7000 ms and 11 TE in the range of 2–2000 ms), and T2* relaxation time using a gradient echo (TR = 1000 ms and seven TE in the range of 2–40 ms) sequences.

Table 1. Spatial and visual cell-amount grading correspondence of SPIO-labeled BMMNCs.* A standardized cardiac segmentation scheme based on the coronary vascular territories (23) was used to determine the segments of interest.

Animal	Segment location	Histology	MRI characterization	MRI characterization
1	5	2	2	2
	6	2	2	2
	11	2	2	2
	12	2	2	2
	16	0	–	–
2	5	0	0	0
	6	2	2	2
	11	0	0	0
	12	0	0	0
	16	0	–	–
3	5	0	0	0
	6	2	2	2
	11	0	0	0
	12	0	0	0
	16	0	–	–

*0 = no cells/label, 1 = a few BMMNCs/slight signal intensity change, 2 = a large amount of BMMNCs/moderate or strong signal intensity change.
–, excluded from analyses.

At 1.5 T (GE Healthcare), TI SE (TR = 500 ms, TE = 13 ms, field of view [FOV] = 200, flip angle [FA] = 90°, number of excitations [NEX] = 1, slice thickness/interval = 3/1.5 mm, and acquisition time [AT] = 5 min 44 s), T2 fast spin echo (FSE) (TR = 5400 ms, TE = 96 ms, FOV = 200 mm, FA = 90°, NEX = 1, slice thickness/interval = 3/1 mm, AT = 3 min 47 s), and T2 fluid-attenuated inversion recovery (FLAIR) (TR = 8802 ms, TE = 133 ms, FOV = 200 mm, FA = 90°, NEX = 1, slice thickness/interval = 3/1.5 mm, AT = 3 min 31 s) sequences were acquired using a four-channel cardiac coil.

In vivo imaging: A 1.5 T scanner (GE Healthcare), a four-channel cardiac coil, and combined ECG and respiratory gating simulating free-breathing were used. Fiesta 2D CINE images were acquired in the vertical long axis, horizontal long axis, and short axis orientations (TR = 4.2 ms, TE = 1.8 ms, matrix size = 256 × 256 mm, view size = 805 × 340 mm, FOV = 340 mm, slice thickness = 8–11 mm). In the short axis orientation, 20 cardiac phases were reconstructed and 30 dynamic images acquired per slice location (the locations covered the left ventricle). A 0.2 mmol/kg gadopentetate dimeglumine (Magnevist, Bayer Healthcare) was injected via the left subclavian vein just prior to (T1, multishot, gradient-echo planar inversion-recovery) the perfusion sequence (TR = 8 ms, TE = 1.2 ms, matrix size = 256 × 256 mm, FOV = 340 mm, slice thickness = 11 mm (3–5 slices). The (segmented inversion

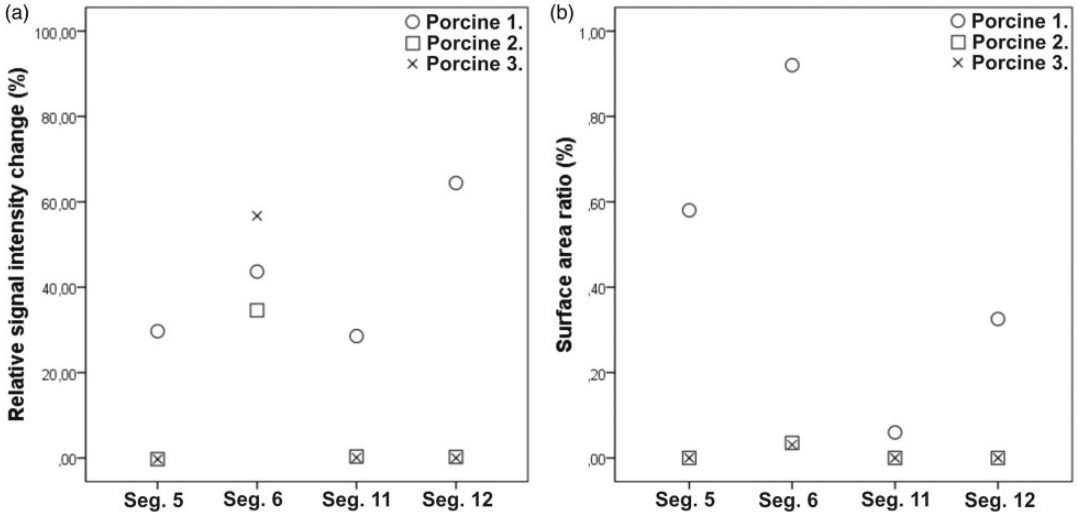

Fig. 2. Quantitative analyses of cell amount in the segments vascularized by CCA. The relative change in signal intensity (signal intensity loss on MRI in each segment caused by SPIO labeled BMMNCs) (a) and surface area ratio (amount of labeled BMMNCs per segment on histology) (b) were compared. The graph shows individual relative change values (open circles, n = 1; open squares, n = 1; and x-symbol, n = 1) of the measured infracted segments.

recovery fast gradient echo) delayed enhancement (DE) sequence (TR = 6.8 ms, TE = 3.2 ms, matrix size = 256 × 256 mm, FOV = 340 mm, slice thickness = 10 mm, TI = 200–150 ms) was performed 10 min after contrast agent injection.

Ex vivo imaging: At 1.5 T (GE Healthcare), a T2* (TE = 15 ms, TR = 660 ms, matrix size = 256 × 256 mm, FOV = 140 mm, slice thickness = 3 mm), and T2 FSE (TE = 86.5 ms, TR = 5400 ms, matrix size = 256 x 256 mm, FOV = 140 mm) sequences were used.

Imaging analyses: In vitro, in vivo, and ex vivo measurements were performed by one investigator trained in radiology and by a radiologist in consensus. The cardiac ejection fraction was measured from 2D CINE images using in-house software (GE advantage workstation AW4.2 (V5.2), GE Healthcare). The amount of myocardium infarcted was evaluated from the 2D CINE (short axis) and DE images (in vivo) and from T2* and T2 FSE images (ex vivo). The cell label visualization was evaluated from 2D CINE (short axis) images (in vivo) and from T2 FSE images (ex vivo). The standardized segmentation scheme was used to identify segmental areas in each slice (24). The extent of AMI was recorded as a number of segments affected. The change in segmental signal intensity caused by the iron label was qualitatively assessed using a three-scale grading: 0 = no change; 1 = slight; 2 = moderate/strong signal intensity change. Quantitative signal changes in myocardium were assessed using the septal, non-affected myocardium as reference. The relative percentage change of signal intensity loss caused by the iron label in each segment was quantitatively calculated from the 2D CINE sequences by using a region of interest (ROI)-based method and by using an open-source viewer software (Osirix v.6.5, Pixmeo, Bernex, Switzerland). The ROI was placed to cover the entire segment and repeated on each slice within the segment during systolic and diastolic phases. The mean value of the segment was used for correlation analysis with histology. The segmental division placed on one slice is presented on Fig. 1. Perfusion and DE sequences were included alongside the 2D CINE sequences to broadly survey label detection and to minimize the possible evaluation problems due to the label artifacts. The altered perfusion was recorded segmentally from perfusion sequences. Of the five segments; 5, 6, 11, 12, 16,

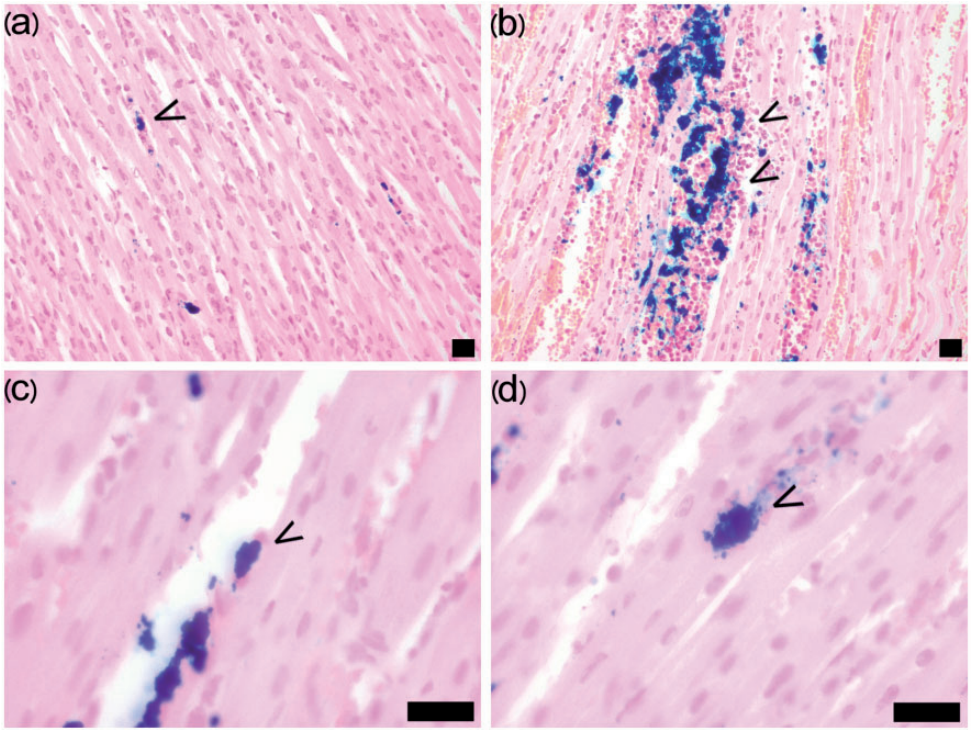

Fig. 3. Number, localization, and morphology of BMMNCs in the myocardium. The number of BMMNCs (arrows) in the myocardium was qualitatively evaluated as: 0 = no cells, 1 = a few cells (a), or 3 = a large amount of cells (b). The BMMNCs mainly localized in slit-like spaces within myocyte bundles or inside vessels or remained in aggregates. (c) Single elongated and flattened cells were situated along the capillary endothelial cells and myocytes in a parallel fashion (arrow). (d) Single cells were also detected among the myocytes (arrow). Prussian blue staining. Scale bar = 20 μm.

vascularized by CCA, the segment most apex, number 16, was excluded from the MRI analysis due to problems in distinguishing the segment volume in MRI.

In vitro, relaxation times acquired at 9.4 T were fitted with exponential relaxation equations using an in-house script (MATLAB, Mathworks Inc., Natick, MA, USA) and assuming mono-exponential decay. Signal intensity in 1.5 T MRI was analyzed by using an open-source viewer software (Osirix v.6.5, Pixmeo). An ROI with a surface of 0.5 cm^2 was manually drawn on each sample and control specimen in order to quantitatively characterize the signal intensity change due to the SPIO label. The signal intensities of labeled specimen were reported as percentage (%) of signal intensities of controls.

Histological analysis

Histological measurements were performed by an investigator trained in histology and a pathologist in consensus. The effect of SPIO labeling on cellular proliferation rate was assessed in vitro by analyzing cultured control cells and labeled BMMNCs with the (3 -(4,5-dimethylthiazol-2-yl)-2,5 -)diphenyltetrazolium bromide assay (Tetrazole, Sigma-Aldrich, St. Louis, MO, USA). MTT absorbance of the cells was measured 1–7 days after labeling by spectrophotometry.

Labeled BMMNCs in the myocardium were analyzed according to the color intensity, shape, and size. The following three-scale classification was used to assess the number of the BMMNCs in the sections within the segments: 0 = no BMMNCs; 1 = a few BMMNCs; and 2 = a large amount of BMMNCs (Table 1). In the final data analysis, the data of each segment was combined so that the grading 1 in more than one section within the segment resulted in a total grade 2.

The scored segments were further quantitatively analyzed by counting the percentage of the surface area covered by labeled cells in each slice by using MCID software (3.0) (Image Analysis Software Solutions for Life Sciences, Interfocus Imaging Ltd., Linton, UK)

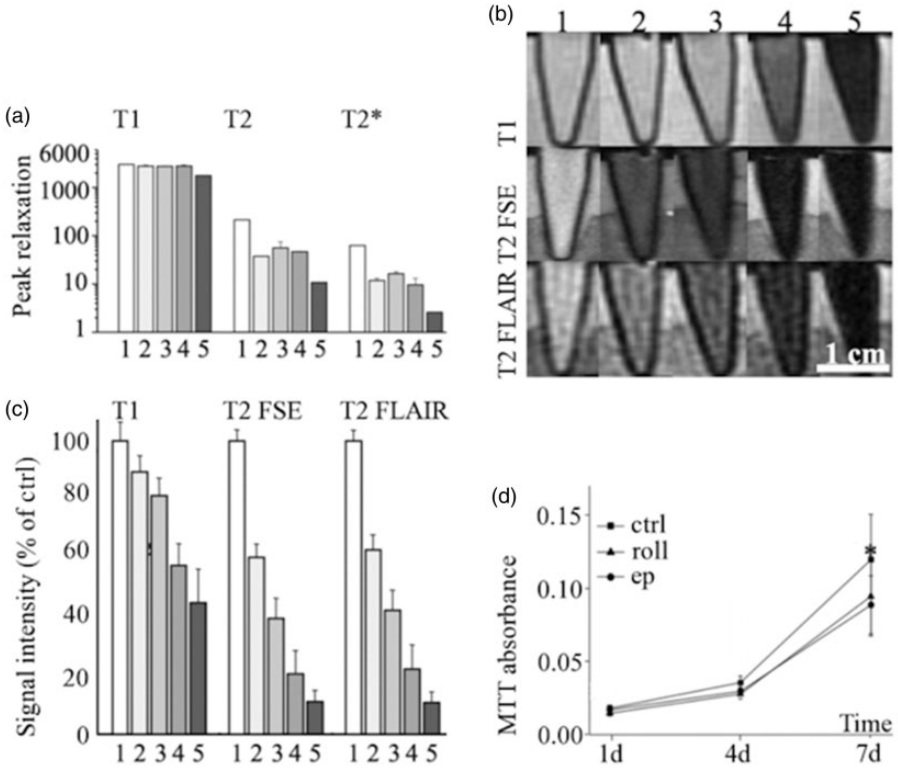

Fig. 4. In vitro measurements of BMMNCs. (a) Peak relaxation measurements at 9.4 T, (b) T1W SE, T2W FSE, and T2W FLAIR images at 1.5 T and (c) relative signal intensity measurements of cells at 1.5 T with the following labeling methods: 1 = control; 2 = 0.1 mg Fe electroporation (100 V, 10 ms); 3 = 0.2 mg Fe electroporation 100 V 5 × 10 ms; 4 = rotating incubation method with 0.1 mg Fe/mL; and 5 = rotating incubation method with 0.2 mg Fe/mL. (d) Proliferation (viability) as measured by MTT absorbance of cells 1–7 days after labeling. The statistically significant difference (< 0.05) is indicated with * = $P < 0.001$. ctrl, control; ep, electroporation; roll, rotating incubation method.

and 20 × magnification. For comparison to the quantitative MRI analysis, the mean percentage of labeled cells in a segment was used (Fig. 2).

Statistical analysis

In vitro data are presented as mean ± standard deviation. Statistical significance was calculated with Student's t-test or one-way analysis of variance (ANOVA) using Origin 8.5 (OriginLab, Northampton, MA, USA).

Results

In the qualitative in vivo MRI analyses, an intramural area of signal loss throughout the whole CINE sequence cardiac cycle was determined to reflect the presence of SPIO-labeled cells and was detected in one to four of the five segments supplied by the CCA in each animal (Fig. 1) corresponding to histology (Table 1). The signal loss was also present in ex vivo MRI images (Fig. 1). There was 100% concurrence between the qualitative MRI and histological grading (Table 1).

In the quantitative in vivo MRI analyses, 24–64% signal intensity loss was detected in the SPIO- containing segments. In the segments where no label was detected on histology, the measured signal intensity change varied from 1% loss to 3% increase. In histology, in the segments containing BMMNCs, the percentage of the surface area covered by BMMNCs was in the range of 0.002–0.927%. The relative change values are presented in Fig. 2.

The mean ejection fraction was 51.9 ± 5%. Delayed enhancement, abnormal perfusion, and abnormal myocardial kinetics indicating AMI were detected in the four segments supplied by the CCA.

In the histological analysis, the majority of BMMNCs displayed no changes in morphology but some had become elongated and flattened and were localized in a parallel fashion along capillary endothelial cells or myocytes as shown in Fig. 3. All the cells adhering to the plastic surface displayed significant intracellular iron granules after 1 h of labeling.

In vitro MRI analyses revealed changed relaxation values at 9.4 T in accordance with the iron content of the samples (Fig. 4). At 1.5 T, the T2W FSE images provided the clearest reduction in observed signal intensity between labeled cells and unlabeled controls (Fig. 4). In the rotating incubation method labeled (0.2 mg Fe/mL) group, there was 89 ± 4% signal reduction on T2W FSE images whereas only 60 ± 7% reduction in signal intensity was detected in the electroporation group.

There was no significant difference between proliferation rate of the SPIO labeled BMMNCs and control cells with either in vitro labeling method, although seven days after the start of culturing, there was a statistically significant difference between the cells labeled by electroporation and control cells ($P < 0.001$) (Fig. 4).

Discussion

In general, the main objective of all cellular MRI techniques is to visualize cells reliably within the target tissue. The current study describes a method for assessing the labeling of BMMNCs both in vitro and in an AMI model.

Here, two novel methods of direct in vitro cell labeling were evaluated in order to validate them for the subsequent in vivo experiment. Previous reports (21,26) have also demonstrated that labeling of cells can be achieved without transfection agents by using carboxydextran-coated SPIO particles. Furthermore, both methods were functionally feasible, achieving rapid 1 h labeling. In previous reports, only magnetoelectroporation has reached a clinically feasible time margin. By increasing the contrast agent dosage, we could further shorten the labelling time, however the high dose of the SPIO label increases the risk of iron oxide aggregation, a problem since the aggregates can pass through filters and be administered into a recipient's bloodstream potentially causing clotting in the microvasculature. In addition, free iron aggregates would introduce less specific imaging.

Our labeling methods exerted no significant effect on cellular viability or proliferation rate (in vitro), which is in accordance with previous reports (27–28).

MRI in vitro showed a clear correspondence between the label and the relaxation rates at 9.4 T. A similar relationship was observed between label concentration and signal intensity changes at 1.5 T. Both methods were functionally feasible and displayed rapid labeling, but the rotating incubation method proved to be more sensitive than electroporation while achieving sufficient signal voids and thus was chosen for in vivo experiments.

In the in vivo experiments, the standardized myocardial segmentation model represented a key element for observation, making possible a retrospective radiological-histological comparison and the segregation of territories vascularized by the CCA and other coronary arteries (24). Hemorrhage is known to have influence on signal decay; however, in histology we did not observe significant hemorrhage and ferritin and hemosiderin concentrations were low. Therefore, the amount of hemorrhage was concluded not to have had a significant impact on signal intensity and thus the signal decrease was concluded mainly to be caused by the

label and not by the hemorrhage. A clear radiological–pathological correlation of cell visualization in both visual and qualitative analyses was observed with 100% sensitivity and specificity. Furthermore, the qualitative cell-count grading comparison displayed an excellent correlation. In our view, these findings reflect the extreme sensitivity of MRI to detect the label and are also in line with previous works with larger animals, where the SPIO-labeled cells were efficiently detected with in vivo MRI (18,19). Our study augments the methodology by introducing a validation protocol for labeling the cells from the in vitro stage to in vivo implementation.

The quantitative MRI analysis appears to be as efficient as a qualitative analysis in detecting the labeled cells; however, we did not detect any significant correlation between the relative signal change in MRI and the label area ratio in histology. We think this discrepancy is likely caused by the difficulty of combining the volumetric datasets originating from MRI to the 2D data of histology. It is noteworthy that histological analyses, both qualitative and quantitative, proved valuable in confirming the presence of labeled cells in tissue. Further studies will be needed to assess the possible use of volumetric histological data for accurately qualifying tissue label content. The extent of the altered ejection fraction was similar between the study animals, suggesting that our MI model was well standardized. This further strengthens the significance of the high spatial correlation of the labeled cells in histology and in MRI morphology. An overall high spatial correspondence was observed between the intramural area of infarction in the in vivo DE and perfusion images, the ex vivo T2W short axis images, and in the gross pathology. In addition to functional changes, DE images revealed persistent hypoenhancement within the hyperenhanced regions, suggesting the presence of persistent microvascular obstruction (PMO) in the area of AMI. PMO has been associated with an increased risk of further cardiac events, poor long-term prognosis, post-infarct complications (29,30), and the extent of PMO has been related to the duration of coronary occlusion (31). Here, the signal loss in DE images was impaired due to the susceptibility artifacts generated by the label, and therefore the extent to which PMO was indeed present remains uncertain. Similar difficulties were also observed in the analysis of the perfusion images. The confounding effects of label are due to the iron oxide particles, which are known to cause changes in the tissue signal similar with naturally occurring endogenous processes such as hemorrhage and macrophage intake of iron (29,32–35). The challenge of MRI quantification of the SPIO label and corresponding number of labeled cells remains as MRI cannot detect cells directly.

The goal of cellular therapy in AMI is to replace the apoptotic myocytes and to modulate inflammatory processes. Our data revealed changes in both localization and morphology, which we interpret as a sign of active migration of BMMNCs and their adherence to endothelial cells and myocytes, findings in line with our previous study, where a cardiac explant culture model was used to study the behavior of injected MSCs and the SPIO label did not influence cellular migration (36).

The major limitations of the present study were the small number of animals and the lack of longitudinal temporal tracking of cells. However, its purpose was to establish the correspondence between imaging and histology in an acute setting and a longitudinal study would not have provided additional information. The variability of methods used can be viewed as a shortcoming but this was inevitable due to the heterogeneity of imaging protocols generally used to perform a clinical cardiac MRI. Importantly, we were able to perform label quantification using both MRI data and histology samples. The lack of control animals in this study is a weakness. However, the cell distribution and migration are likely to differ because of hemorrhaging, edema, and hypo-perfusion and thus control animals without AMI would not be appropriate comparisons as the goal of the work was to evaluate the distribution and migration of cells in the acute phase of AMI.

In conclusion, SPIO labeling for imaging purposes is possible by novel yet simple methods—the rotating incubation method and electroporation. MRI can achieve both accurate detection and quantification of SPIO labeled cells in a large-animal AMI model.

Declaration of conflicting interests

The author(s) declared no potential conflicts of interest with respect to the research, authorship, and/or publication of this article.

Funding

The author(s) disclosed receipt of the following financial support for the research, authorship, and/or publication of this article: This study has received funding from the Sigrid Jusélius Foundation.

References

1. Yusuf S, Hawken S, Ounpuu S, et al. Effect of potentially modifiable risk factors associated with myocardial infarction in 52 countries (the INTERHEART study): case-control study. Lancet 2004;364:937–952.
2. Reddy K, Khaliq A, Henning RJ. Recent advances in the diagnosis and treatment of acute myocardial infarction. World J Cardiol 2015;7:243–276.
3. Krause U, Harter C, Seckinger A, et al. Intravenous delivery of autologous mesenchymal stem cells limits infarct

size and improves left ventricular function in the infarcted porcine heart. Stem Cells Dev 2007;16:31–37.
4. Mäkelä J, Ylitalo K, Lehtonen S, et al. Bone marrow derived mononuclear cell transplantation improves myocardial recovery by enhancing cellular recruitment and differentiation at the infarction site. J Thorac Cardiovasc Surg 2007;134:565–573.
5. Orlic D, Kajstura J, Chimenti S, et al. Bone marrow cells regenerate infarcted myocardium. Nature 2001;410: 701–705.
6. Alestalo K, Korpi R, Mäkelä J, et al. High number of transplanted stem cells improves myocardial recovery after AMI in a porcine model. Scand Cardiovasc J 2015;49:82–94.
7. Jeevanantham V, Butler M, Saad A, et al. Adult bone marrow cell therapy improves survival and induces long-term improvement in cardiac paramets: a systematic review and meta-analysis. Circulation 2012;126:551–568.
8. Wollert KC, Meyer GP, Ltz J, et al. Intracoronary autologous bone-marrow cell transfer after myocardial infarction: the BOOST randomized controlled clinical trial. Lancet 2004;364:141–148.
9. Uccelli A, Moretta L, Pistoia V. Mesenchymal stem cells in health and disease. Review. Nat Rec Immunol 2008;8: 726–736.
10. Makino S, Fukuda K, Miyoshi S, et al. Cardiomyocytes can be generated from marrow stromal cells in vitro. J Clin Invest 1999;103:697–705.
11. Pittenger MF, Mackay AM, Beck SC, et al. Multilineage potential of adult human mesenchymal stem cells. Science 1999;284:143–147.
12. Beeres SL, Bengel FM, Bartunek J, et al. Role of imaging in cardiac stem cell therapy. J Am Coll Cardiol 2007;49: 1137–1148.
13. Graham JJ, Lederman RJ, Dick AJ. Magnetic resonance imaging and its role in myocardial regenerative therapy. Regen Med 2006;1:347–355.
14. Weissleder R, Cheng HC, Bogdanova A, et al. Magnetically labeled cells can be detected by MR imaging. JMRI 1997;7:258–263.
15. Bulte JW, Kraitchman DL. Iron oxide MR contrast agents for molecular and cellular imaging. NMR Biomed 2004;17:484–499.
16. Malliaras K, Smith RR, Kanazawa H, et al. Validation of contrast-enhanced magnetic resonance imaging to monitor regenerative efficacy after cell therapy in a porcine model of convalescent myocardial infarction. Circulation 2013;128:2764–2775.
17. Kraitchman DL, Kedziorek DA, Bulte JWM. MR imaging of transplanted stem cells in myocardial infarction. Methods Mol Biol 2011;680:141–512.
18. Ma GS, Qi C, Liu N, et al. Efficiently tracking of stem cells in vivo using different kinds of superparamagnetic iron oxide in swine with myocardial infarction. Chin Med J 2011;124:1199–1204.
19. He G, Zhang H, Wei H, et al. In vivo imaging of bone marrow mesenchymal stem cells transplanted into myocardium using magnetic resonance imaging: A novel method to trace the transplanted cells. Int J Cardiol 2007;114:4–10.
20. Fu Y, Kraitchman DL. Stem cell labelling for noninvasive delivery and tracking in cardiovascular regenerative therapy. Expert Rev Cardiovasc Ther 2010;8: 1149–1160.
21. Walczak P, Kedziorek DA, Gilad AA, et al. Instant MR labeling of stem cells using magnetoelectroporation. Magn Reson Med 2005;54:769–774.
22. Hsiao J, Tai M, Chu H. Magnetic nanoparticle labeling of mesenchymal stem cells without transfection agent: cellular behavior and capability of detection with clinical 1.5 t magnetic resonance at the single cell level. Magn Reson Med 2007;58:717–724.
23. Mäkelä J, Anttila V, Ylitalo K, et al. Acute homing of bone marrow-derived mononuclear cells in intramyovardial vs. intracoronary transplantation. Scand Cardiovasc J 2009;43:366–373.
24. Cequiera MD, Weissman NJ, Dilsizian V, et al. Standardized myocardial segmentation and nomenclature for tomographic imaging of the heart: A statement for healthcare professionals from the Cardiac Imaging Committee of the Council on Clinical Cardiology of the American Heart Association. Circulation 2002;105: 539–542.
25. de Vries MA, Harrison A. Physical chemistry: Model's reputation restored. Nature 2010;16:908–909.
26. Mailänder V, Lorenz MR, Holzapfel V. Carboxylated superparamagnetic iron oxide particles label cells intracellularly without transfection agents. Mol Imaging Biol 2008;10:138–146.
27. Arbab AS, Yocum GT, Wilson LB, et al. Comparison of transfection agents in forming complexes with ferumoxides, cell labeling efficiency, and cellular viability. Mol Imaging 2004;3:24–32.
28. Suzuki Y, Zhang S, Kundu P, et al. In vitro comparison of the biological effects of three transfection methods for magnetically labeling mouse embryonic stem cells with ferumoxides. Magn Reson Med 2007;57: 1173–1179.
29. Tallheden T, Nannmark U, Lorentzon M, et al. In vivo MR imaging of magnetically labeled human embryonic stem cells. Life Sci 2006;9:999–1006.
30. Hombach V, Grebe O, Merkle N, et al. Sequelae of acute myocardial infarction regarding cardiac structure and function and their prognostic significance as assessed by magnetic resonance imaging. Eur Heart J 2005;26: 549–557.
31. Choi SH, Kang JW, Kim ST, et al. Investigation of T2-weighted signal intensity of infracted myocardium and its correlation with delayed enhancement with reperfused acute myocardial infarction. Int J Cardiovasc Imaging 2009;25:111–119.
32. Mani V, Adler E, Briley-Saebo KC, et al. Serial in vivo positive contrast MRI of iron oxide-labeled embryonic stem cell-derived cardiac precursor cells in a mouse model of myocardial infarction. Magn Reson Med 2008;60:73–78.
33. Ansalem Y, Mardor Y, Feinberg MS, et al. Iron-oxide labeling and outcome of transplanted mesenchymal stem cells in the infracted myocardium. Circulation 2007;116: 138–145.

34. Terrovitis J, Stuber M, Youssef A, et al. Magnetic resonance imaging overestimates ferumoxide-labeled stem cell survival after transplantation in the heart. Circulation 2008;117:1555–1562.
35. Pawelczyck E, Jordan EK, Balakumaran A, et al. In vivo transfer of intracellular labels from locally implanted bone marrow stromal cells to resident tissue macrophages. PLoS One 2009;214:e6712.
36. Alestalo K, Lehtonen S, Yannopoulos F, et al. Activity of mesenchymal stem cells in a nonperfused cardiac explant model. Tissue Eng Part A 2013;19:1122–1131.